

## Rheological properties of poly(lactic acid) based nanocomposites: Effects of different organoclay modifiers and compatibilizers

Eda Acik,<sup>1</sup> Nese Orbey,<sup>2</sup> Ulku Yilmazer<sup>1</sup>

<sup>1</sup>Chemical Engineering Department, Middle East Technical University, Ankara 06800, Turkey

<sup>2</sup>Chemical Engineering Department, University of Massachusetts, Lowell, Massachusetts 01854

Correspondence to: N. Orbey (E-mail: nese\_orbey@uml.edu)

**ABSTRACT:** Poly(lactic acid) (PLA) nanocomposites containing five types of organically modified, layered silicates and two elastomeric compatibilizers, namely ethylene-glycidyl methacrylate (E-GMA) and ethylene-butyl acrylate-maleic anhydride (E-BA-MAH), were prepared using a twin screw extruder. The morphologies of the nanocomposites were determined by X-ray diffraction (XRD) and transmission electron microscopy (TEM), and the rheological properties of the melts were measured using small-amplitude oscillatory shear. XRD revealed that the addition of E-GMA to the binary nanocomposites resulted in higher compatibility between the organoclay nanoplatelets and the polymer matrix. TEM showed that all of the nanocomposites contained mixed dispersed structures, involving tactoids of various sizes, as well as intercalated and exfoliated organoclay layers. Rheological properties were found to be affected by the differences in the compatibility between the organoclays and the polymer matrix, and by the addition of the compatibilizer. Organoclay types that resulted in high level of dispersion exhibited higher values of complex viscosity compared to that of neat PLA. The addition of E-GMA introduced a solid-like rheological behavior at low frequencies. All of the nanocomposites had similar rheological behavior at high frequencies. © 2015 Wiley Periodicals, Inc. *J. Appl. Polym. Sci.* **2016**, *133*, 42915.

**KEYWORDS:** clay; composites; rheology

Received 19 September 2014; accepted 4 September 2015

DOI: 10.1002/app.42915

### INTRODUCTION

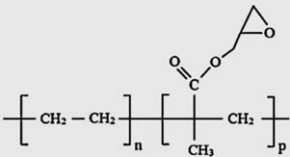
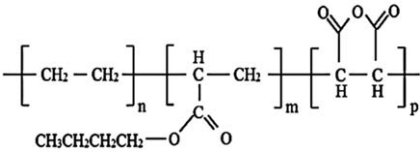
Poly(lactic acid) (PLA) is biodegradable and is thus of interest owing to its environmental advantages, but its commercial applications are limited by its low fracture toughness. Copolymerization,<sup>1,2</sup> plasticization,<sup>3,4</sup> the addition of organic or inorganic fillers,<sup>1,5</sup> and melt blending with ductile polymers<sup>6,7</sup> are some of the methods that have been proposed to improve its mechanical properties. Utilization of nanosized fillers are very popular and promising, however, it has been found that the nanofillers often reduce elongation at break and impact strength. These negative effects can be overcome by the use of a third component, for example a flexible polymer.<sup>8</sup> However, the incorporation of a flexible polymer into a brittle polymer such as PLA, while toughening the product, also causes reductions in tensile strength and modulus.<sup>9</sup> Coupling the advantages of nanofillers and flexible polymers is a promising approach for the optimization of the mechanical properties of the resulting ternary system.

The rheological behavior of the nanocomposite systems is of interest because of its importance in processing and as a tool for characterizing structure, morphology, and filler dispersion

when used along with other techniques. There are a number of studies on the rheological behavior of binary and ternary PLA nanocomposites. Di *et al.*<sup>10</sup> investigated binary PLA/organoclay nanocomposites using (2–10 wt %) Cloisite 30B (C30B) as the nanofiller and observed higher values of complex viscosity  $\eta^*$ , storage modulus ( $G'$ ), and loss modulus ( $G''$ ) compared with those of pure PLA. Even at the lowest filler loading (2 wt %), the Newtonian plateau disappeared at low frequencies. These findings were mainly attributed to the strong interaction between C30B and PLA molecules, as well as the effective dispersion of the filler in the polymer matrix. Singh *et al.*<sup>11</sup> studied the rheological behavior of the same nanocomposite combination, PLA/C30B. Increases in the values of  $\eta^*$ ,  $G'$ , and  $G''$  were observed as the organoclay content increased. Increases in the moduli and viscosity values were attributed to an interconnected structure and reinforcement of the molten PLA by C30B, owing to hydrogen bonding of the hydroxyl groups in the organic modifier of the organoclay and carbonyl groups of the PLA chains.

The rheological behaviors of ternary PLA nanocomposites have been also studied. Bhatia<sup>12</sup> examined the rheological behavior and thermal properties of ternary PLA, poly(butylene succinate)

**Table I.** Structures of Compatibilizers

Compatibilizer	Chemical structure	Content
Lotader <sup>®</sup> AX8840 (E-GMA)		8 wt % GMA
Lotader <sup>®</sup> 2210 (E-BA-MAH)		2.6 wt % MAH 8 wt % BA

(PBS), and C30B nanocomposites. At a constant PLA/PBS ratio, the limit of the linear viscoelastic region decreased with increasing organoclay concentration. The storage modulus of the PLA/PBS blend was always higher than that of nanocomposites with low filler content (1–3 wt %) over the entire frequency range (0.1–100 rad/s). Similar trends were observed for  $G''$  and  $\eta^*$ , and the authors attributed this to minimal interparticle interactions compared to the systems with higher organoclay content. Ternary blends of PLA with poly [(butylene succinate)-*co*-adipate] (PBSA) and organoclay having several PLA/PBSA ratios and 3 wt % clay were studied by Eslami and Kamal.<sup>13</sup> Oscillatory shear experiments revealed strong solid-like behavior for the systems with more than 50 wt % PBSA. This was attributed to large numbers of clay platelets at the PLA/PBSA interface, resulting in polymer-particle and particle-particle network-like structures.

Most studies of the rheology of PLA-based binary or ternary organoclay nanocomposites have been limited to the effects of the nanofiller content and blending ratio. There has been little consideration of the effects of the modifier structure. Krikorian and Pochan<sup>14</sup> studied the effects of modifier miscibility and extent of clay modification on the overall nanocomposite formation with three commercial organophilic clay types (Cloisites<sup>®</sup> 15A, 25A, and 30B), using the solution-intercalation film-casting method. From the morphological results, they concluded that the degree of miscibility of the organic modifier with PLA was the key factor for filler dispersion. This was supported by computation of the solubility parameters. C30B was selected as the most suitable organoclay for good dispersion and exfoliation, owing to the favorable enthalpic interaction between the diols in its organic modifier and C=O bonds in the PLA backbone. Pluta *et al.*<sup>15</sup> studied the effects of the filler concentration, clay modifier, and plasticization using three modified clays (C20A, C25A, and C30B) with poly(ethylene glycol)-plasticized PLA. Intercalation of the silicate layers was shown to depend on the structure of organic modification. Among the three organoclays, C30B was most prone to intercalate the plasticized PLA matrix. The stronger interaction of PLA with C30B was thought to be due to hydrogen bonding between the carbonyl group in the main chain of the PLA molecules and the hydroxyl group in the organic modifier of C30B.<sup>10</sup>

As aforementioned, studies on the effects of the modifier structure in PLA/organoclay binary and ternary nanocomposites are limited. This article describes the effects of organoclays and compatibilizers on the morphology of PLA nanocomposites and their rheological properties under oscillatory shear. This work is a part of a larger study on increasing the toughness and processability of PLA by incorporating elastomeric compatibilizers with epoxy and maleic anhydride (MAH) functionalities and organically modified clays. Five organically modified commercial clays were used as nanofillers at low concentrations, since the structure of the modifier is the key parameter in PLA/organoclay nanocomposites. In addition, two elastomers with different functional groups (ethylene glycidyl methacrylate [E-GMA] and ethylene butyl acrylate (BA)-maleic anhydride [E-BA-MA]) were used as compatibilizers to study the effects of the elastomeric phase. The clay and compatibilizer contents were kept constant to focus attention on the effects of the structure of the additives on the rheological and morphological properties of the resultant nanocomposites.

## EXPERIMENTAL METHODS

### Materials

A transparent, injection molding grade PLA with 5% d-lactide stereoisomer content, weight average molecular weight ( $M_w$ ) of 278 g/mol and polydispersity index ( $M_w/M_n$ ) of 1.78 was purchased from NaturePlast, France. A random copolymer of ethylene (E) and GMA, Lotader<sup>®</sup> AX8840, and a terpolymer of ethylene (E), BA, and MAH, Lotader 2210, were obtained from Arkema Chemicals, France to be used as the compatibilizer. Five montmorillonites: Cloisites<sup>®</sup> 15A (C15A), 25A (C25A), and 30B (C30B), and Nanofils<sup>®</sup> 5 and 8 (N5 and N8), modified with various quaternary ammonium salts, were purchased from Southern Clay Products, TX. The structures of the compatibilizers and modifiers are shown in Tables I and II, respectively. The structures of the modifiers in C15A, N5, and N8 are the same, but their concentrations are different in each organoclay type.

### Nanocomposite Preparation

Nanocomposites were prepared by melt blending in a corotating, intermeshing Thermoprism TSE 16 TC twin screw extruder ( $L = 384$  mm,  $D = 16$  mm) that contained kneading elements.

**Table II.** Structures and d-Spacings of Organic Modifiers

Organoclay	Modifier structure	d-Spacing (Å)
Cloisite <sup>®</sup> 15A	$\begin{array}{c} \text{CH}_3 \quad \text{Cl}^- \\   \\ \text{H}_3\text{C} - \text{N}^+ - \text{HT} \\   \\ \text{HT} \end{array}$	33.1
Cloisite <sup>®</sup> 25A	$\begin{array}{c} \text{CH}_3\text{SO}_4^- \quad \text{CH}_3 \\   \quad   \\ \text{H}_3\text{C} - \text{N}^+ - \text{CH}_2\text{CHCH}_2\text{CH}_2\text{CH}_2\text{CH}_3 \\   \quad   \\ \text{HT} \quad \text{CH}_2 \\   \\ \text{CH}_2 \end{array}$	18.3
Cloisite <sup>®</sup> 30B	$\begin{array}{c} \text{CH}_2\text{CH}_2\text{OH} \\   \\ \text{H}_3\text{C} - \text{N}^+ - \text{T} \quad \text{Cl}^- \\   \\ \text{CH}_2\text{CH}_2\text{OH} \end{array}$	18.0
Nanofil <sup>®</sup> 5	$\begin{array}{c} \text{CH}_3 \quad \text{Cl}^- \\   \\ \text{H}_3\text{C} - \text{N}^+ - \text{HT} \\   \\ \text{HT} \end{array}$	33.1
Nanofil <sup>®</sup> 8	$\begin{array}{c} \text{CH}_3 \quad \text{Cl}^- \\   \\ \text{H}_3\text{C} - \text{N}^+ - \text{HT} \\   \\ \text{HT} \end{array}$	36.4

HT: hydrogenated tallow.

The screw speed was 250 rpm, and the barrel temperature was 170°C. Prior to extrusion, all of the raw materials were dried overnight under vacuum. Drying temperatures were 85°C for PLA and organoclays, and 70°C for E-GMA and E-BA-MAH. The extrudate was pelletized for use in injection and compression molding samples for morphology analyses and rheological measurements, respectively. Neat PLA (unfilled) was also melt-processed under the same shear and thermal conditions to be used as the reference material. Melt processed materials were kept in desiccators at all times to prevent hydrolysis of PLA by moisture. To observe the effects of the various compatibilizers and organoclays, their loadings in the polymer matrix were kept constant at 10 and 2 wt %, respectively.

### Sample Preparation

The morphology of the nanocomposites was studied using injection molded samples prepared with a laboratory scale injection-molding machine (DSM Micro 10 cc Injection Molding Machine). The barrel and mold temperatures were 170 and 55°C, respectively, and the maximum pressure was 12 bars. For rheological measurements, the samples were compression molded at 180°C using a laboratory press. The compression molding procedure was comprised of 5 min warm-up period, followed by repeated compression/decompression cycles to eliminate the trapped air bubbles. The samples were then cooled to room temperature under low pressure and removed from the mold after the temperature dropped below the  $T_g$  of the polymer. Since PLA is highly moisture sensitive, samples were dried in vacuum oven overnight and stored in a desiccator prior to use. Storage time was kept to a minimum and was the same for all of the samples.

### Characterization

**X-ray Diffraction (XRD).** XRD patterns of organoclays and nanocomposites were obtained using a Rigaku Ultima-IV X-Ray diffractometer that generates a voltage of 40 kV and current 40 mA from a Cu K $\alpha$  radiation source ( $\lambda = 1.5418 \text{ \AA}$ ). The diffraction angle,  $2\theta$ , was scanned from 1° to 10° at a scanning rate of 1°/min and a step size of 0.01°. Injection molded samples, 2 mm thick, were analyzed.

**Transmission Electron Microscopy.** The nanoscale morphologies of the PLA nanocomposites were examined using high resolution transmission electron microscopy (FEI, Tecnai G2 F30) operated at an accelerating voltage of 300 kV. For TEM imaging, ultrathin sections ( $\sim 120 \text{ nm}$ ) were prepared from injection molded samples with a cryogenic ultramicrotome (Leica, EMFC6) that operated at  $-80^\circ\text{C}$ .

**Rheological Measurements.** The linear viscoelastic behavior of PLA nanocomposite melts was determined using oscillatory shear. Compression molded samples of 20 mm in diameter and 3 mm thick were kept in desiccators before measurements. An ARES G2 Rheometer was used with parallel disk fixtures. The parallel disks were 25 mm in diameter, therefore the compression molded samples were squeezed to a diameter of 25 mm, thus covering the entire area of the disks. Any small amount of excess material was wiped out. Thus, all the materials were subjected to the same thermomechanical history. The melt stability of the nanocomposites was determined by time sweeps at fixed frequency and strain amplitude. In order to determine the limit of linear viscoelastic behavior, strain sweep measurements were performed at strains of 0.1–100% at a frequency of 10 rad/s at 170°C. All subsequent frequency sweep measurements were

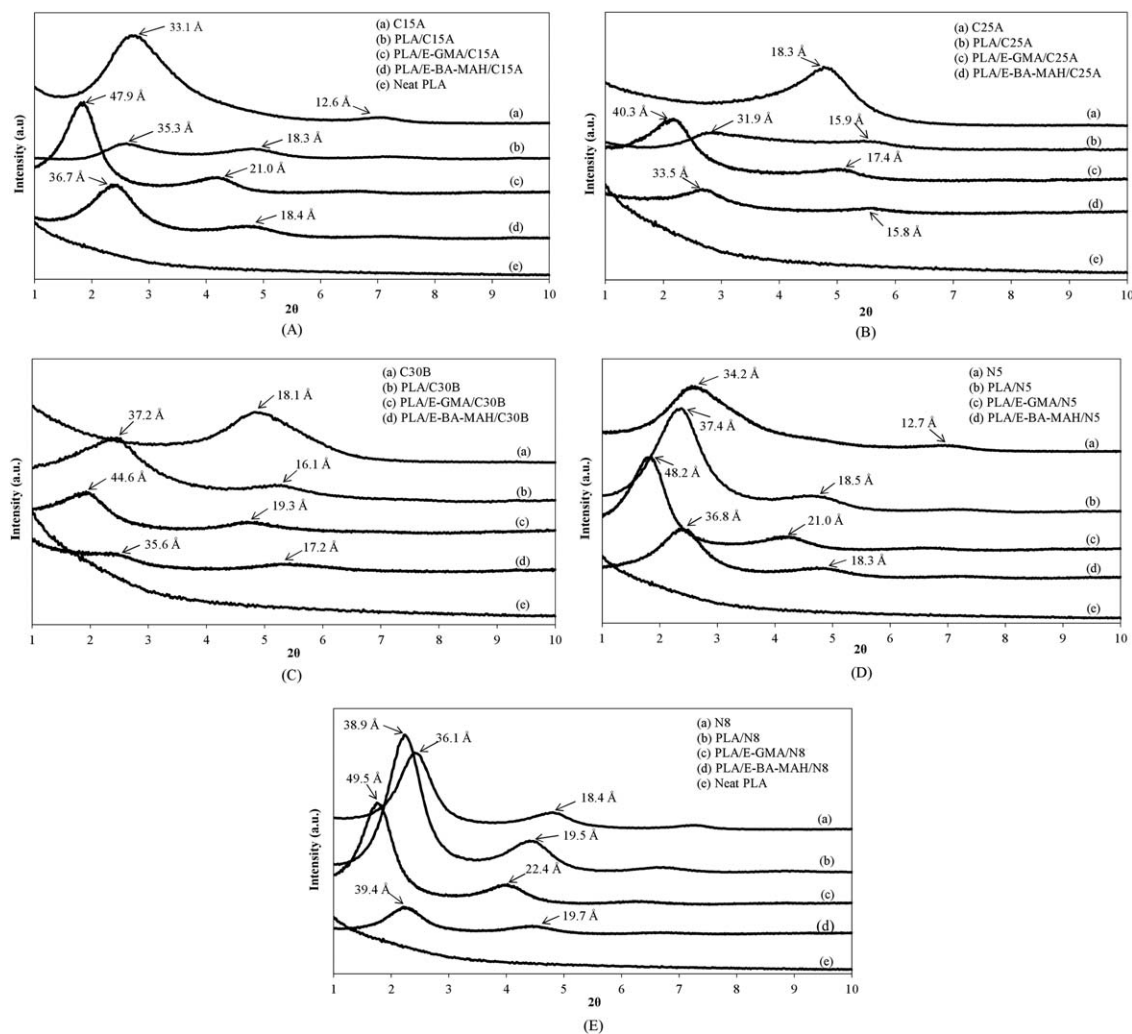


**Figure 1.** XRD patterns for PLA nanocomposites filled with different organically modified organoclays (A) C15A, (B) C25A, (C) C30B, (D) N5, and (E) N8.

carried out at between 0.1 and 500 rad/s and at constant strain amplitude of 5%, which was found to be well within the linear region. To ensure that there was no significant thermal degradation, a time sweep was also carried out at the test temperature.

## RESULTS AND DISCUSSION

### XRD Analyses

XRD patterns of the nanocomposites in the range of  $2\theta = 1\text{--}10^\circ$  revealed the interlayer spacing ( $d$ ) between the silicate layers of organoclays. The interlayer spacing was calculated by Bragg's law:  $d = \lambda/n/(2\sin\theta)$ . A left-shift in the peak indicates an increase in the interlayer spacing of the silicate layers, whereas the disappearance of a characteristic peak can be an indication of exfoliated structure or poor dispersion of the clay.<sup>8</sup> In this case, we wanted to back the XRD results by using TEM. The TEM results indicate high level of exfoliation. Figure 1 shows the XRD patterns of the binary and ternary nanocomposites as well as those of neat PLA and organoclays. Neat PLA showed no reflection peaks in the scanned range. The basal spacings of the organoclay powders were 33.1, 18.3, 18.1, 34.2, and 36.1 Å

for C15A, C25A, C30B, N5, and N8, respectively. Under the same processing conditions, each type of organoclay had a different degree of intercalation indicating that the chemical compatibility between the polymer matrix and the organoclay is the most important parameter governing the final morphology. Other parameters, such as the applied shear stress, residence time in the extruder, and process temperature, affected only the size of the organoclay tactoids.<sup>16</sup>

Peak shifts were more apparent for the nanocomposites prepared with C25A [Figure 1(B)] and C30B [Figure 1(C)]. Previous studies have compared the affinities of C25A and C30B for PLA, showing that C30B has high affinity for this polymer matrix.<sup>13,14</sup> Changes in the  $d$ -spacing values calculated from the XRD patterns in this study were in accordance with the reports in the literature. PLA/C30B reached a gallery height of 37.2 Å, compared to 18.1 Å for pure C30B powder, and PLA/C25A reached 31.9 Å, compared with 18.3 Å for pure C25A. The addition of compatibilizer altered the peak positions, especially for E-GMA. For PLA/E-GMA/C25A, the peak showing a basal spacing of 18.3 Å was shifted to 40.3 Å, and a second peak

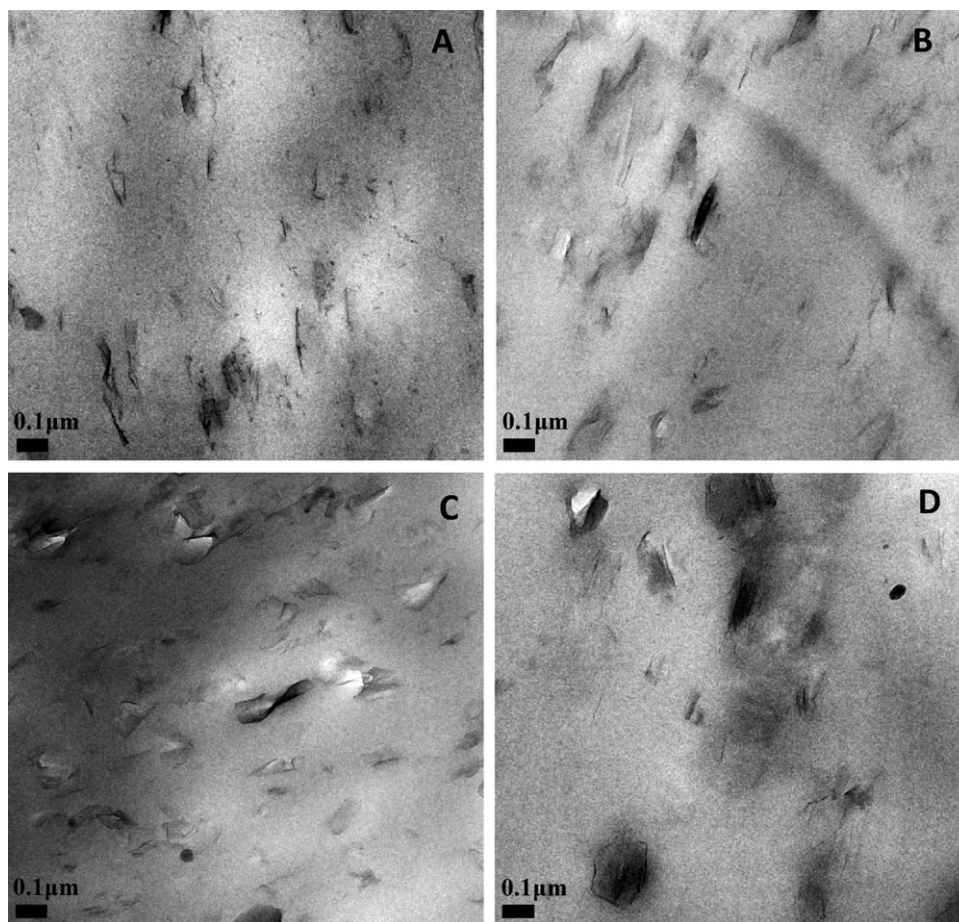


**Figure 2.** Low magnification TEM micrographs of the nanocomposites containing 2 wt % clay: (A) PLA/C25A; (B) PLA/E-GMA/C25A; (C) PLA/N5; (D) PLA/E-GMA/N5.

showing a basal spacing of 17.4 Å, appeared due to unintercalated organoclay. A smaller shift was seen in the interlamellar space of PLA/E-BA-MAH/C25A (33.5 Å). Among the Cloisites, C30B has the lowest and C15A the highest hydrophobicity. The high hydrophobicity of C15A resulted in a low degree of intercalation according to the XRD patterns. In addition, the XRD patterns of nanocomposites containing C15A, N5, and N8 had similar traces. These three organoclays contain the same modifier (Table II). Changes in the gallery heights of nanocomposites containing these three clay types were lower than those of the C25A and C30B. For some nanocomposites (i.e., PLA/C15A, PLA/C25A, and PLA/E-GMA/C25A), the intensities of the characteristic peaks were lower than those of neat organoclay. However, none of the nanocomposites exhibited a clear disappearance of the basal reflection peak. The decrease in intensities can be attributed to the presence of mostly exfoliated structure, since in general, delamination of the silicate layers prevents X-ray diffraction from the layers resulting in the disappearance of the diffraction peaks.<sup>8</sup> The diffraction peaks of some of the samples had higher intensities than the pure organoclay powders (i.e., pure N8 and PLA/N8 nanocomposite). For the nanocomposites lower intensities were anticipated, because the nanocomposites contained only 2 wt % organoclay. However, the nature of the sample affects the XRD patterns, and the

nanocomposites were analyzed as injection-molded samples, whereas the pure organoclays were in powder form. The preferred orientation of crystallites in solid samples may disappear in the powder form.<sup>17</sup> However, in some samples the organoclay layers were intercalated, but still retained an ordered structure.

#### TEM Analyses

Although XRD is a good method for determining the changes in the spacing of silicate layers, it does not provide enough information on the spatial distribution of the organoclay nanoparticles and possible structural inhomogeneity in the nanocomposites.<sup>8,18</sup> Thus, high-resolution TEM was used to understand these discrepancies and the interactions between polymer, compatibilizer, and organoclay. Four samples were selected for TEM imaging. This selection was made on the basis of the XRD patterns and the rheological data (discussed in the following section). Nanocomposites of C25 and N5 were selected for TEM analysis, but the samples containing E-BA-MAH as the rubbery phase were not studied. This choice was made for two reasons. First, the interlayer spacing of the organoclay was not increased in the presence of E-BA-MAH, and the rheological properties were not enhanced. Second, although not within the scope of this report, the mechanical properties of the nanocomposites containing E-BA-MAH were not

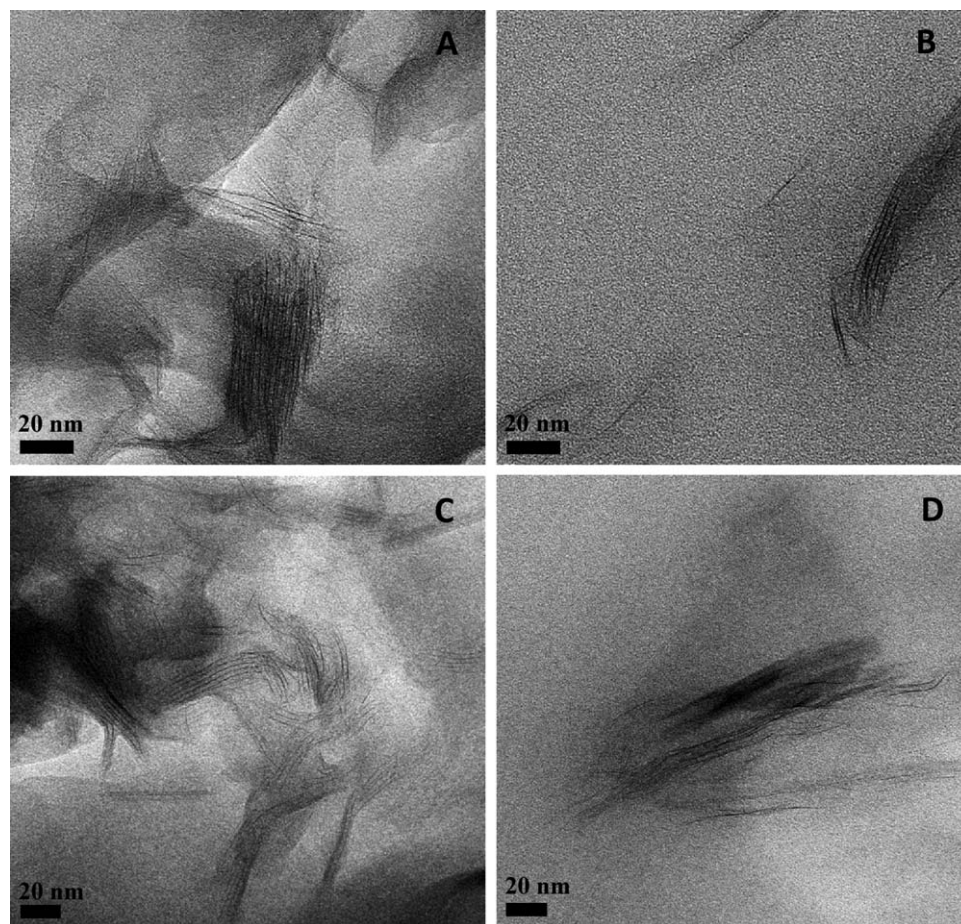


**Figure 3.** High magnification TEM micrographs of the nanocomposites containing 2 wt % clay: (A) PLA/C25A; (B) PLA/E-GMA/C25A; (C) PLA/N5; (D) PLA/E-GMA/N5.

enhanced compared to those of neat PLA. Figure 2 shows bright field images of the selected nanocomposites at low magnification. Because of the low contrast difference between the polymer matrix and the rubbery phase, the positions of the organoclay nanoplatelets could not be exactly determined. The XRD patterns suggest that the addition of E-GMA increased the interlayer spacing. Thus, the organoclay nanoplatelets are most likely to be embedded in the E-GMA phase or positioned at the interface. Baouz *et al.*<sup>18</sup> studied the effects of mixing protocols on impact modified PLA layered silicate nanocomposites. Their system was very similar to the one studied here. They concluded that the clay layers are mostly located in the rubbery phase, mainly because the rubbery phase melted at a lower temperature and encapsulated the clay layers. The organoclay nanoplatelet dispersions were homogeneous, but the stack sizes were variable. In particular, the stacks of C25A were smaller than the stacks of N5, especially in the presence of E-GMA. Figure 3 shows high-magnification TEM images of the same nanocomposites. Although the sizes of the organoclay stacks at low magnification changed with the type of organoclay, the structures of the dispersed organoclay nanoplatelets were similar at high magnification. All of the nanocomposites showed mixed organoclay dispersion, with partial exfoliation, intercalation, and small tactoids appearing in all the images.

### Linear Viscoelastic Behavior

**Thermal Stability of Samples.** Figure 4 shows the storage moduli of processed neat PLA and its blends as functions of time. After 10 min, the storage moduli decreased from their initial values by 16, 6, and 12% for PLA, PLA/E-GMA, and PLA/E-BA-MAH, respectively, indicating that blending with the compatibilizers had a positive effect on the thermal stability. Decreases

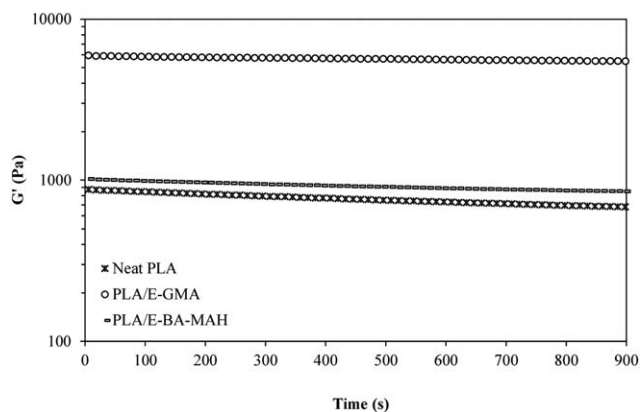


**Figure 4.** Time sweep data of processed neat PLA, and PLA/E-GMA and PLA/E-BA-MAH blends at 170°C, 5% strain amplitude and 10 rad/s.

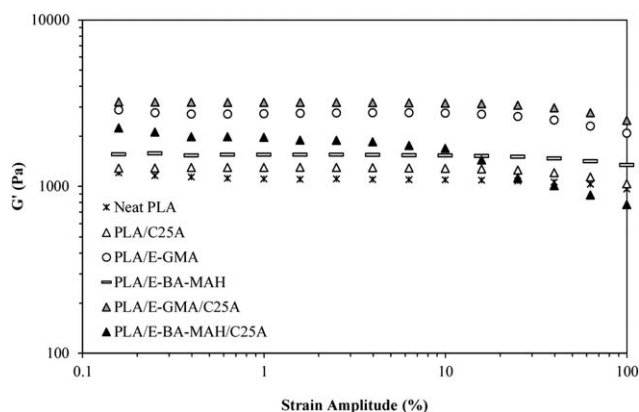


**Figure 5.** Strain sweep data of processed neat PLA, PLA/compatibilizer blends, and binary and ternary nanocomposites produced with C25A.

in the storage modulus values of PLA and PLA blends are thought to be acceptable when thermal stabilizer is not used.<sup>19,20</sup> The decreases in the storage modulus curves of the layered silicate-filled nanocomposites were smaller (data not shown) owing to the increased thermal stability of polymer-layered silicate nanocomposites.<sup>21,22</sup> Consequently, to ensure that samples had a stable viscoelastic response, the frequency sweeps studied later were limited to 10 min for a given sample.

**Strain Sweep Measurements.** Strain sweeps are used to determine the range of linear viscoelastic behavior. Figure 5 shows strain sweep curves of neat PLA and its binary and ternary nanocomposites for one organoclay type (C25A) as an example. Similar trends were observed for all of the organoclay types. The small increase at the lowest strain amplitude probably results from reduced precision due to the very low torque values in this region. The range of linear behavior extends to 10%, and our measurements that follow were made at strain amplitude of 5%. In the linear range, the applied strain was insufficient to disturb the microstructure. Compared to simple nanocomposites, the blends and ternary nanocomposites had higher storage modulus values, and they exhibited more obvious nonlinear behavior. In particular, PLA/E-BA-MAH/C25A showed an abrupt change in the limit of nonlinearity compared with its binary combinations. Nanocomposites with different types of organoclays were similarly investigated. All of the nanocomposites showed a similar trend in the limit of linearity, but with different orders of magnitude of rheological properties.

**Frequency Sweep Measurements.** Frequency sweep measurements were performed at a common strain amplitude (5%), at which all of the nanocomposites were within their LVR. As mentioned before, the frequency sweeps were limited to 10 min during which the samples had a stable viscoelastic response. Polyesters are prone to thermal degradation during processing. Degradation issues in PLA and polyethylene terephthalate–nanoclay composites were addressed in recent publications.<sup>23–25</sup> For PLA, various chain extenders were used to compensate for chain scission and the rheological behavior was analyzed.<sup>23,24</sup> Ghanbari *et al.* developed a correlation to correct for the thermal degradation that may take place during testing.<sup>25</sup> In this work,

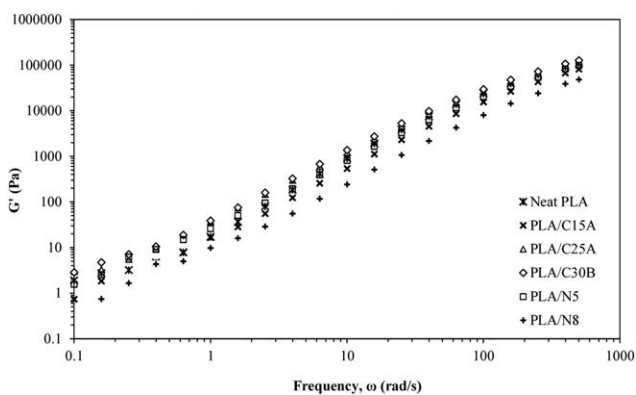


**Figure 6.** Storage modulus as a function of frequency for PLA/organoclay nanocomposites produced with different types of organoclays.

we wanted to ensure that all samples including the neat PLA were subjected to the same thermal and shear history. To this end, as explained in the experimental section, neat PLA as well all of the nanocomposite samples were melt processed under the same conditions. Similarly, the sample preparation and testing conditions for the oscillatory shear experiments were the same for all the samples.

Figures 6 and 7 show the  $G'$  and complex viscosity data of the PLA nanocomposites with different organoclays. All of the nanocomposites showed the same trend, but small differences were apparent that provide information on the modifier–matrix interactions. There were no significant differences in the slopes of the curves in Figure 6 compared with those of processed neat PLA. It has been reported in the literature that at high filler loadings (above 5%), owing to the formation of a network structure,  $G'$  may become independent of the frequency at low frequencies, indicating solid-like behavior.<sup>10,12</sup> However, at the low filler loading used in the current study (2 wt %), the storage moduli of the nanocomposites do not significantly show this effect. Only the storage modulus of nanocomposites containing C25A and C30B are slightly higher than that of neat PLA. The compatibility of these organoclays with the polymer matrix is supported by the XRD patterns obtained in this study and previous studies.<sup>13,14</sup> Thus, these organoclays exhibit the highest intercalation and highest  $G'$  among the organoclays studied in this investigation. The storage modulus of the

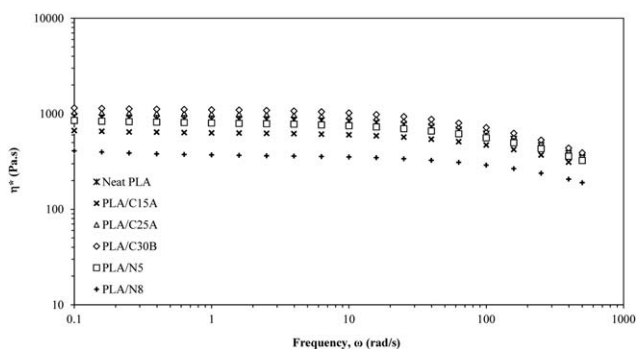


**Figure 7.** Complex viscosity as a function of frequency for PLA/organoclay nanocomposites produced with different types of organoclays.

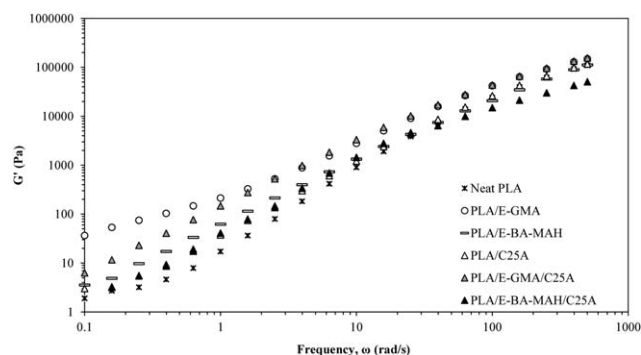
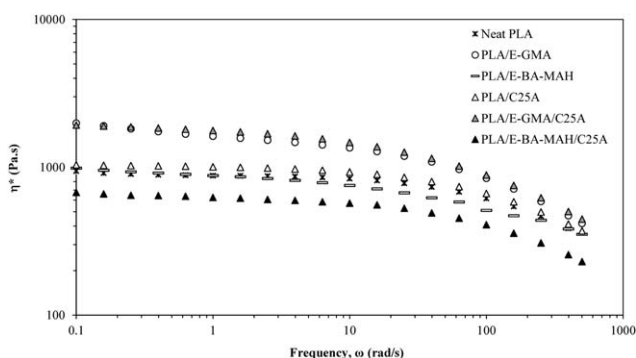


**Figure 8.** Storage modulus as a function of frequency for neat PLA, PLA/compatibilizer blends, and binary and ternary nanocomposites produced with C25A.

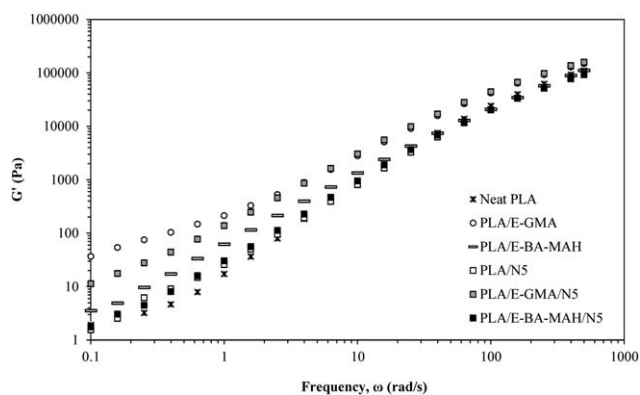
nanocomposite with N5 is very close to that of neat PLA. However, the  $G'$  values of nanocomposites with C15A and N8 are lower than those of PLA at all frequencies, owing to the lowest degree of intercalation observed among the organoclays studied.

Figure 7 shows the complex viscosities of the binary PLA nanocomposites. Typically, the addition of fillers would increase melt viscosity, as was observed for the C30B and C25A nanocomposites that showed the highest degree of intercalation. Even though the increases of the complex viscosities of the nanocomposites prepared with these two clays are incremental, they are apparent compared to the other clay types. The complex viscosities of nanocomposites with C15A, N5, and N8, are lower than that of pure PLA, since these nanocomposites exhibit low degrees of intercalation. The last three organoclays have the same modifier structures used at different content. At low organoclay loadings, it was observed that the complex viscosity of the nanocomposite may be lower than that of the neat polymer which was explained with the limited interparticle interactions.<sup>12,25</sup>

Based on the rheological behavior of the binary nanocomposites, the organoclay types can be classified into two groups. C25A and C30B produced higher interaction with the polymer matrix with higher degrees of intercalation resulting in higher storage modulus and complex viscosity compared to C15A, N5, and N8. However, C15A, N5, and N8 yielded lower degrees of



**Figure 9.** Complex viscosity as a function of frequency for neat PLA, PLA/compatibilizer blends, and binary and ternary nanocomposites produced with C25A.



**Figure 10.** Storage modulus as a function of frequency for neat PLA, PLA/compatibilizer blends, and binary and ternary nanocomposites produced with N5.

intercalation and lower complex viscosities. In nanocomposites with C15A, N5, and N8, the incompatibility of the modifier-matrix system may result in stacks of silicate layers that would align easily even at low frequencies. This possibility was supported by the findings with low-magnification TEM showing that organoclay stacks of N5 are larger than those of C25A.

A third phase was added to both groups of organoclays for two reasons. First, the third phase is expected to act as a compatibilizer between the organoclay surface and the polymer matrix. Second, in practical applications the presence of a properly selected additional phase can lead to enhanced mechanical properties. In this study, the effects of adding two different types of compatibilizers were examined for C25A and N5 nanocomposites. Figure 8 shows the storage moduli of the nanocomposites containing C25A. To follow the step-by-step effects of adding both the filler and the compatibilizer, the data of neat PLA and its binary blends are also shown. In the low-frequency region, the PLA/E-GMA blend and its nanocomposite resulted in considerably higher modulus values in comparison to the storage modulus of neat PLA. In particular, the slope of the PLA/E-GMA blend at low frequencies changed drastically exhibiting solid-like behavior. The addition of organoclay to the PLA/E-GMA blend reduced the solid-like behavior. In the presence of organoclay, the interaction between PLA and compatibilizer could be limited due to the preferential placement of the silicate layers on the interface of the matrix polymer and the elastomeric phase. In the PLA/E-BA-MAH blend, the solid-like behavior was not very marked; the storage modulus of this blend was even lower than that of PLA/E-GMA/C25A nanocomposite. This result might be due to the higher reactivity of the epoxide group of GMA towards the functional end groups of PLA (hydroxyl and carboxyl groups) compared to the reactivity of the MAH functional group. A decrease in  $G'$  in the low-frequency region was also seen with the addition of C25A to the PLA/E-BA-MAH blend. In the high-frequency region, the  $G'$  values were quite similar for all the nanocomposites (Figure 8). This result indicates that the addition of organoclay had no substantial influence on the short-range dynamics of the blend, and that the chain relaxation modes were almost independent of the presence of the silicate layers.<sup>11,26</sup>



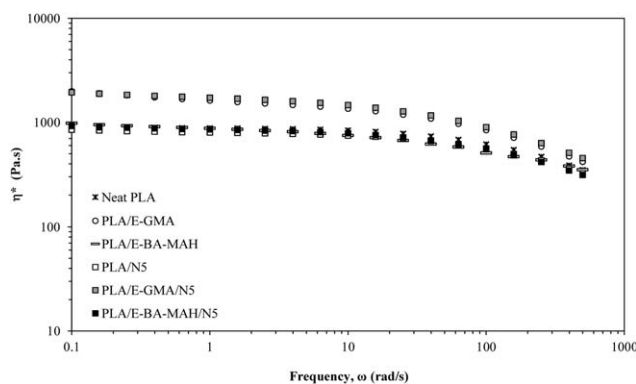


**Figure 11.** Complex viscosity as a function of frequency for neat PLA, PLA/compatibilizer blends, and binary and ternary nanocomposites produced with N5.

The complex viscosity curves (Figure 9) exhibited comparable modulus values at high frequencies, supporting the previous interpretation. PLA/E-BA-MAH/C25A has the lowest complex viscosity, whereas the complex viscosity of the PLA/E-BA-MAH blend is almost the same as that of PLA. The reason for this might be the increased chain mobility and easy alignment of the silicate layers due to weak interactions in the PLA/E-BA-MAH/C25A ternary system. On the other hand, PLA/E-GMA and its nanocomposite exhibit high complex viscosity throughout the entire frequency range, that can be attributed to the higher compatibility of E-GMA with PLA and the successful reactive blending achieved in melt extrusion. Enhanced complex viscosity could be attributed to flow restrictions resulting from strong interactions in the PLA/E-GMA system.

Even though the degree of organoclay dispersion is different, the N5 nanocomposites exhibit qualitatively similar storage modulus behavior as the C25A nanocomposites (Figure 10). The solid-like behavior of the PLA/E-GMA blend was reduced with the addition of organoclay, and the storage moduli of all the other samples are below the storage modulus of PLA/E-GMA. Storage modulus data reach approximately the same values in the high frequency region, indicating that the relaxation of the matrix polymer is not significantly affected by the layered silicates. The complex viscosity data of the N5 nanocomposites (Figure 11) also reflect the effect of the compatibilizer. Presence of N5 in the PLA/E-GMA blend did not significantly alter the viscosity behavior. Considering the complex viscosities, when successful reactive blending is achieved as in the case of PLA/E-GMA systems, the effect of blending suppresses the effect of organoclay modifier compatibility at the low filler content used in this study. The most explicit effect of compatibilizer and filler addition was seen in storage modulus at low frequencies for all samples.

## CONCLUSIONS

The effects of different organoclays and compatibilizers on the morphology of PLA nanocomposites and their rheological properties under oscillatory shear were investigated. It was shown the dispersion of nanoclay in the PLA matrix is strongly affected by the type of organic modifier in the organoclay. Although all the nanocomposites had both intercalated and exfoliated layers

with some tactoids, the degree of intercalation was governed by the chemical compatibility between the polymer matrix and the modifier. The structure of the compatibilizer also affected the final morphology. High degrees of intercalation were obtained between C25A and C30B and the compatibilizer E-GMA due to matching polarity and the high reactivity of the epoxide group in E-GMA with the end groups of PLA, possibly resulting in a network structure in the final product. Changes in the microstructure were reflected in the rheological properties. The strongest shear-thinning was observed for the nanocomposites containing E-BA-MAH due to weak interactions between MAH and PLA. The binary PLA/organoclay nanocomposites exhibited enhanced dynamic properties only for the nanocomposites with strong interactions as shown by the XRD patterns. The addition of E-GMA to PLA introduced a distinct solid-like behavior to PLA at low frequencies. The solid-like behavior of PLA/E-GMA blend was reduced by the addition of organoclay, possibly due to positioning of the organoclay layers in the ternary nanocomposites. All of the nanocomposites showed similar rheological behaviors at high frequencies, which shows that the chain relaxation modes are not affected by the 2 wt % clay loading.

## ACKNOWLEDGMENTS

The authors are grateful for the financial support from TUBITAK International Research Fellowship Program 2214-A for supporting Dr. Eda Acik during her work at the University of Massachusetts, Lowell. They would like to thank Dr. Robert Malloy and Dr. Margaret Sobkowicz-Kline, Plastics Engineering Department of University of Massachusetts Lowell for helpful discussions and for the use of their facilities. They would also like to thank Nathanael Effendy for his help with sample preparation.

## REFERENCES

- Grijpma, D. W.; Nijenhuis, A. J.; van Wijk, P. G. T.; Pennings, A. J. *Polym. Bull.* **1992**, *29*, 571.
- Hiljanen-Vainio, M.; Karjalainen, T.; Seppälä, J. *J. Appl. Polym. Sci.* **1996**, *59*, 1281.
- Sinclair, R. G. *J. Macromol. Sci. A* **1996**, *33*, 585.
- Baiardo, M.; Frisoni, G.; Scandola, M.; Rimelen, M.; Lips, D.; Ruffieux, K.; Wintermantel, E. *J. Appl. Polym. Sci.* **2003**, *90*, 1731.
- Ray, S. S.; Maiti, P.; Okamoto, M.; Yamada, K.; Ueda, K. *Macromolecules* **2002**, *35*, 3104.
- Anderson, K. S.; Lim, S. H.; Hillmyer, M. A. *J. Appl. Polym. Sci.* **2003**, *89*, 3757.
- Li, Y.; Shimizu, H. *Macromol. Biosci.* **2007**, *7*, 921.
- Ray, S. S.; Okamoto, M. *Prog. Polym. Sci.* **2003**, *28*, 1539.
- Liu, H.; Zhang, J. *J. Polym. Sci. Part B: Polym. Phys.* **2011**, *49*, 1051.
- Di, Y.; Iannace, S.; Maio, E. D.; Nicolais, L. *J. Polym. Sci. Part B: Polym. Phys.* **2005**, *43*, 689.
- Singh, S.; Ghosh, A. K.; Maiti, S. N.; Raha, S.; Gupta, R. K.; Bhattacharya, S. *Polym. Eng. Sci.* **2012**, *52*, 225.
- Bhatia; Gupta, R. K.; Bhattacharya, S. N.; Choi, H. J. *J. Appl. Polym. Sci.* **2009**, *114*, 2837.

13. Eslami, H.; Kamal, M. R. *J. Appl. Polym. Sci.* **2013**, *129*, 2418.
14. Krikorian, V.; Pochan, D. J. *Chem. Mater.* **2003**, *15*, 4317.
15. Pluta, M.; Paul, M. A.; Alexandre, M.; Dubois, P. *J. Polym. Sci. Part B: Polym. Phys.* **2006**, *44*, 299.
16. Marras, S. I.; Zuburtikudis, I. *J. Appl. Polym. Sci.* **2012**, *124*, 2999.
17. Morgan, A. B.; Gilman, J. W. *J. Appl. Polym. Sci.* **2003**, *87*, 1329.
18. Baouz, T.; Rezgui, F.; Yilmazer, U. *J. Appl. Polym. Sci.* **2013**, *128*, 3193.
19. Palade, L. I.; Lehermeier, H. J.; Dorgan, J. R. *Macromolecules* **2001**, *34*, 1384.
20. Corre, Y. M.; Duchet, J.; Reignier, J.; Maazouz, A. *Rheol. Acta* **2011**, *50*, 613.
21. Alexandre, M.; Dubois, P. *Mater. Sci. Eng.* **2000**, *28*, 1.
22. Sinha Ray, S.; Bousmina, M. *Prog. Mater. Sci.* **2005**, *50*, 962.
23. Najafi, N.; Heuzey, M. C.; Carreau, P. J.; Wood-Adams, P. M. *Polym. Degrad. Stab.* **2012**, *97*, 554.
24. Najafi, N.; Heuzey, M. C.; Carreau, P. J. *Compos. Sci. Technol.* **2012**, *72*, 608.
25. Ghanbari, A.; Heuzey, M. C.; Carreau, P. J.; Ton-That, M. T. *Rheol. Acta* **2013**, *52*, 59.
26. Zhao, H.; Cui, Z.; Wang, X.; Tung, L. S.; Peng, X. *Compos. B* **2013**, *51*, 79.